From cylinder to city: How recondensation-induced nucleation in vehicle exhaust shapes urban aerosol number

Jen-Ping Chen[1,2,3], I-Chun Tsai[3], Li-Wei Kuo[1], Gong-Do Hwang[4]

[1]Department of Atmospheric Sciences, National Taiwan University, Taipei City, Taiwan

[2]International Degree Program in Climate Change and Sustainable Development, National Taiwan University, Taipei City, Taiwan

[3]Research Center for Environmental Changes, Academia Sinica, Taipei City, Taiwan

[4]NVIDIA Singapore

Correspondence to: Jen-Ping Chen (jpchen@ntu.edu.tw)

Abstract. Air-quality models frequently underestimate fine particle number concentration (PNC), particularly in the nucleation/Aitken range—while reproducing $PM_{2.5}$ mass more accurately, suggesting that key number-forming processes are missing from current frameworks. We propose and investigate a physically motivated pathway, Recondensation-Induced Nucleation (RIN), in which pre-existing ambient aerosols are vaporized during combustion and subsequently re-nucleate as the exhaust cools, selectively boosting particle number with negligible impact on mass.

Controlled four-stroke engine experiments demonstrate that a distinct nucleation mode (<30 nm) appears only when ambient aerosols are present in the intake air, providing direct laboratory evidence of RIN. Parcel-model simulations of H_2SO_4–H_2O systems further examine particle evaporation under in-cylinder condition and the self-limiting nature of nucleation. A parameterized RIN module was implemented in the Community Multiscale Air Quality (CMAQ) model and evaluate under Taiwan/West-Pacific urban conditions. Without RIN, CMAQ underpredicted PNC by 75% and overpredicted $PM_{2.5}$ by 21% at the Xitun urban site; incorporating RIN reduced the PNC bias to 22% with negligible change in $PM_{2.5}$. The RIN mechanism thus transfers accumulation-mode mass to Aitken-mode number, not only partially alleviates the low-PNC bias but also the low Aitken- to accumulation mode number ratio bias found at the Xitun site. While RIN improves PNC estimates, it also leads to overestimation at the smallest sizes, likely reflecting inherent limitations in the modal parameterization.

1. Introduction

The impact of aerosols on human health is a major concern in air pollution research. A growing body of evidence shows that mass concentration is not the sole or most appropriate measure of potential health effects, implying that health studies must consider other characteristics, such as particle number, particle morphology, and detailed chemical speciation (Mauderly 1993, 1999; Glovsky 1997; Albritton and Greenbaum 1998). Epidemiological and toxicological research indicates that the particle number concentration (PNC), especially of ultrafine particles (UFPs, <100 nm), has a more substantial effect on

human health than mass concentration (Oberdürster 2000; Chung et al. 2015; Li et al. 2016b). Due to their diminutive size, UFPs contribute less to mass than larger particles but can penetrate deep into the respiratory system and even enter the bloodstream, leading to inflammation as well as respiratory and cardiovascular diseases (Pope III and Dockery 2006). For the same amount of mass, a high PNC also implies a large surface area, which leads to stronger toxicity and chemical reactivity with body molecules (Oberdörster et al. 2005; Balmes and Hansel 2024). Several recent studies have highlighted the importance of PNC as a critical metric for assessing air pollution's health impacts (e.g., Kelly and Fussell 2020; Schraufnagel 2020; Schwarz et al. 2023; Stafoggia et al. 2023).

Air quality and atmospheric chemistry modeling remains a crucial tool for both scientific research and policy-making concerning atmospheric aerosols. Modern models can now simulate the aerosol particle size distribution (PSD), which is a crucial property for assessing aerosol impact on human health and climate. While PNC is derived from this distribution, recent studies have found that models often underestimate PNC (Xausa et al. 2018; Fanourgakis et al. 2019; Leinonen et al. 2022; Kohl et al. 2023; Wang et al. 2023; Kim et al. 2025), particularly in the nucleation and Aitken modes. Such underestimation arises from various factors, including but not limited to limitations in emission inventories (Wang et al. 2023), emission PSD (Park et al. 2006; Spracklen et al. 2010; Sartelet et al. 2022), missing/weak nucleation pathways (Kusaka et al. 1995; Yu 2001; Sorokin et al. 2004; Dunne et al. 2016; Wang et al. 2023; Shao et al. 2024), simplifications in various microphysical processes (Chen et al. 2011; Mann et al. 2012; Westervelt et al. 2013; Chen et al. 2021; Patoulias and Pandis 2022), and numerical methods (Mann et al. 2012; Jacquot and Sartelet 2025).

In air-quality simulations over urban areas—where health impacts are of greatest concern—the underestimation of particle number concentration (PNC) may not primarily stem from weak or missing atmospheric nucleation pathways. New particle formation (NPF) tends to be weak in environments, such as the study area, where substantial pre-existing aerosol concentrations act as strong condensation sinks for precursor vapors (Dal Maso et al. 2002; Manninen et al. 2010; Jeong et al. 2010; Qi et al. 2015; Salma et al. 2016), and can even be largely suppressed under heavily polluted conditions (Guo et al. 2014; Gani et al. 2020). Under the heavily polluted conditions frequently encountered in the study area, classical atmospheric nucleation pathways therefore play a limited role in controlling PNC. Consistent with this interpretation, neither the measurements nor the air-quality simulations presented below reveal significant NPF events. Moreover, the other potential explanations discussed above likewise lack direct observational verification as the dominant cause of PNC underestimation in urban environments.

Among these potential model deficiencies, this study investigated a new particle production mechanism proposed by Chen (1999), which is related to both emission and nucleation in urban areas. This Recondensation-Induced Nucleation (RIN) mechanism suggests that aerosols pre-existing in the intake air may be vaporized during engine combustion, and the vapors thus generated may produce strong nucleation during cooling of the exhaust air. Chen (1999) provided supporting experimental evidence by heating up ambient air through a high-temperature furnace and then immediately cooling it down, revealing a strong production of UFP at the expense of existing accumulation-mode aerosol particles.

Several studies have suggested that the RIN mechanism may contribute to contrail formation from cryoplanes, which do not

emit combustion aerosols because they burn liquid hydrogen (Ström and Gierens 2002; Gierens et al. 2008; Lee et al. 2010). The mechanism has also been invoked to explain anomalous increases in particle number observed in dilution tunnel experiments (Lombaert et al. 2006). Beyond these specific contexts, however, systematic mechanistic investigation of RIN —and its implications for air quality—has remained limited. This scarcity of research highlights a significant gap in our understanding of RIN as a potentially important particle formation pathway. It is important to note that the furnace experiment by Chen (1999) did not involve real combustion, which itself can generate UFPs, limiting the direct applicability of those results to air quality modeling. Accordingly, a primary objective of the present study is to extend the RIN concept to more realistic conditions by conducting controlled engine combustion experiments with and without ambient aerosols in the intake air. We further evaluate the atmospheric relevance of RIN by parameterizing the laboratory findings and implementing them in a regional air-quality model to assess their impact on urban particle number concentrations.

The paper is structured as a hierarchical, scale-bridging framework that progresses from controlled laboratory evidence to mechanistic understanding and, ultimately, to atmospheric-scale implications. The engine-exhaust experiments in Section 2 establish the empirical foundation by demonstrating the critical role of ambient aerosols in new particle formation under realistic combustion conditions. These findings motivate the idealized air-parcel simulations in Section 3, which translate the experimental conditions into a mechanistic framework that explicitly resolves particle evaporation during heating and nucleation during subsequent cooling. The parcel model explains the observed relationship between ambient aerosol loading and the resulting PNC, and further examines the effects of incomplete particle evaporation. Insights gained from both the experiments and parcel simulations are then synthesized into a RIN parameterization implemented in the CMAQ regional air-quality model in Section 4. This final step assesses the atmospheric relevance of RIN by evaluating whether a mechanism identified at the laboratory scale can account for the long-standing underestimation of PNC in urban simulations without substantially altering $PM_{2.5}$ mass.

2. Engine Combustion Experiments

To investigate the RIN mechanism under realistic combustion conditions, we conducted controlled engine-exhaust experiments under three intake configurations—Amb-In, Pur-In, and Lad-In—and measured PSD (11.5–453 nm) in the exhaust with a TSI SMPS 3934.

2.1 Experimental setup

The most common motor vehicles in the urban areas of East and Southeast Asian countries are gasoline-engine motorcycles (including scooters) and passenger cars. For example, motorcycles account for approximately 60–65% of registered vehicles in Taiwan, and their proportion is similarly high in the studied area of Taichung City. In addition, motorcycles contribute disproportionately to urban emissions due to their large numbers, frequent stop-and-go operation, and high activity in near-road environments. According to the latest Taiwan Emission Data System (TEDS 11.0/12.0), motorcycles are a primary

contributor to urban air pollution, accounting for nearly 40% of total $PM_{2.5}$ emissions in the Taichung City. Because testing high-displacement passenger-car engines on our bench was impractical, we used a four-cylinder motorcycle engine for the combustion experiments.

The combustion experiments were conducted with intake air under controlled aerosol conditions, according to the schematic shown in Fig. 1. We consider three types of experiments: (1) Intake of ambient air (Amb-In), (2) Intake of purified air (Pur-In), and (3) Intake of artificial aerosol-laden air (Lad-In). The Amb-In versus Pur-In contrast isolates and demonstrates the RIN mechanism under realistic conditions, extending the conceptual experiment of Chen (1999). As Chen (1999) suggested that the intensity of new particle formation via RIN depends on pre-existing particle loading, the Lad-In experiments were designed to explicitly test this dependence by varying the seed aerosol mass/number.

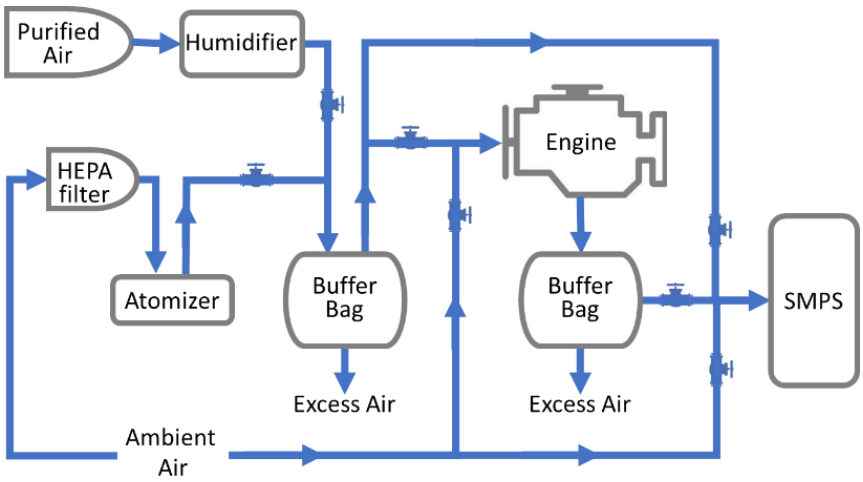

Figure 1. Engine-exhaust experiment flow paths (Amb-In / Pur-In / Lad-In) with SMPS sampling; blue arrows indicate flow; valves and buffer bags annotated.

To provide intake air for experiment Pur-In, we applied laboratory-grade purified air and verified its particle-free status prior to use. We also considered using a high efficiency-particulate air (HEPA) filter for removing particles, but rejected this option because condensable gases (e.g., ammonia and nitric acid) can pass through and influence nucleation in the exhaust air. To mimic ambient moisture, the purified air was humidified to ~85% relative humidity (*RH*) by passing it through a 4.0 mol kg^{-1} salt solution before entering the engine.

For the Lad-In experiments, the intake air was first filtered with a HEPA filter and then seeded with aerosol generated from ammonium sulfate solution (in deionized water). Unlike the Pur-In case, residual condensable gases upstream are not critical here because the loaded aerosol evaporates in-cylinder, producing far greater amounts of condensable vapors that drive nucleation upon cooling. The seed solution had a molality of 4.455 mol kg^{-1}, chosen to be roughly in equilibrium with ~85% RH. Particles were produced with a TSI 9302 Single Jet Atomizer, yielding a modal diameter of ~100 nm (cf. Fig. S1).

Ammonium sulfate was selected to represent local aerosol composition (prevalent in the study region) and because its neutralized, less corrosive nature (relative to sulfuric acid) enables safer handling. The PNC introduced into the engine was controlled by diluting the aerosol with purified air. All intake-air streams (Amb-In, Pur-In, and Lad-In) were temporarily held in a 200 L buffer bag for flow stabilization before entering the combustion engine. Buffer bags and tubing were replaced frequently to prevent cross-contamination, and each bag was purged with filtered air at the start of every experiment.

The combustion platform was a 100 cc, four-stroke motorcycle engine with electronic fuel injection (EFI) operated at a steady 2000 rpm. The engine was warmed for 20 min before each run to reach thermal and emissions steady state. Peak burned-gas temperatures in such engines typically reach ~1700–2600 K during ignition and combustion of the air–fuel mixture (Shehata 2010; Mosburger et al. 2013; Heywood, 2018), although temperature at the cylinder walls and piston surface is much lower, often controlled to about 450 K in car engines due to cooling systems. These temperatures far exceed the nominal boiling point of sulfuric acid (~444.7 K) and the decomposition/vaporization threshold of ammonium sulfate (~510 ± 20 K), enabling partial to near-complete in-cylinder evaporation of pre-existing particles. The subsequent exhaust cooling thus favors RIN.

The PSDs were measured with a TSI SMPS 3934 over 11.5–453 nm. In our earlier experiments, particle sampling was conducted directly in the open air behind the tailpipe; however, the measured concentrations exhibited considerable fluctuations due to pressure pulsations from the engine cylinder and turbulent mixing with ambient air. To reduce this variability, the exhaust was routed into a buffer bag and then drawn continuously into the SMPS. In this revised setup, the exhaust air primarily cools through conduction along the walls of the exhaust pipe, buffer bag, and sampling tubes, while mixing with ambient air was minimized and not considered in the analysis. Each experiment was repeated multiple times (n = 7 for Experiments 1 and 2; n ≥ 4 for each case in Experiment 3), and we report the run-averaged PSDs. Ambient PSDs were measured immediately before and after each experiment to document background conditions.

2.2 Experimental results

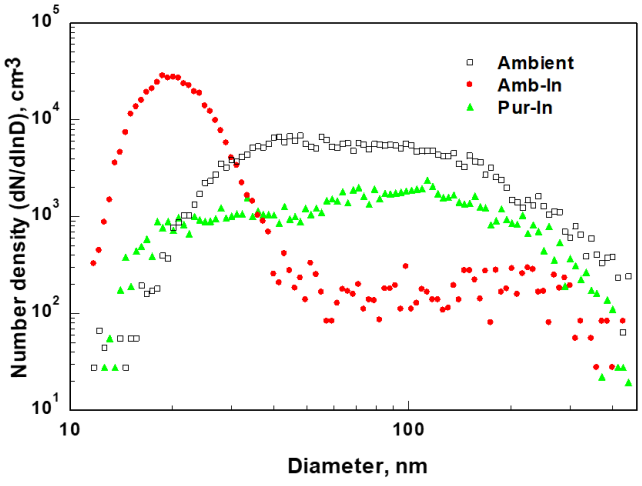

Figure 2: Comparison of PSD for Amb-In (red dots), Pur-In (green triangles), and ambient intake-air (black squares) treatments. Amb-In shows distinct <30 nm nucleation mode and reduced accumulation number.

The Amb-In vs. Pur-In comparison (Fig. 2) clearly demonstrates the RIN mechanism: PNC in Amb-In is substantially higher than in Pur-In, and the Amb-In PSD exhibits a prominent nucleation mode (< ~30 nm). In Pur-In, particles in the exhaust are expected to consist primarily of combustion residuals (e.g., soot and organic fragments). These particles are unlikely to be ambient particles introduced through mixing or leakage, as the buffer-bag design prevents entrainment of outside air into the system. A small fraction of fuel sulfur (~10 ppm by mass) may oxidize to H_2SO_4 (e.g., Sorokin et al. 2004; Fleig et al. 2013), but the feeble nucleation mode observed in Pur-In indicates that fuel-sulfur-driven nucleation is minor under our conditions. In contrast, Amb-In introduces pre-existing ambient aerosol that evaporates in-cylinder and re-nucleates as the exhaust cools, yielding the strong nucleation-mode peak and, notably, a marked reduction of accumulation-mode number relative to ambient air. This pattern is consistent with mass-to-number conversion via RIN—i.e., condensation of evaporated material onto many newly formed small particles rather than onto fewer, larger ones.

We also note that the accumulation-mode number in Amb-In is lower than in Pur-In, even though both conditions should generate soot. This could reflect suppressed soot formation (e.g., altered flame chemistry or cooling rates in the presence of evaporating ambient aerosols) or subtle procedural differences (e.g., flow paths indicated in Fig. 1). Disentangling these possibilities requires targeted diagnostics and is left for future work.

The Lad-In experiments show that exhaust PNC increases with intake aerosol loading (Fig. 3), corroborating Chen (1999) that RIN-driven particle production depends on the abundance of pre-existing aerosols. However, the output PNC varies by only about one order of magnitude despite a three-order-of-magnitude change in input loading. This muted response likely reflects (i) a baseline soot contribution present across all loadings that dilutes the apparent RIN sensitivity, (ii) self-limiting nucleation: as numerous new particles form, enhanced condensation and coagulation sinks suppress further number growth (Lehtinen et al. 2007; Tuovinen et al. 2022), and (iii) the limitation in certain nucleation pathways, chemiion–mediated nucleation (Yu et al 2004). In addition, at very high loadings, incomplete in-cylinder evaporation of the seeded aerosol may cap the vapor available for re-nucleation, further weakening the scaling. We examine these two factors with parcel-model simulations in the next section.

Notably, exhaust PNCs in the Lad-In experiments exceed those in Amb-In. Beyond differences in experimental plumbing and ambient conditions (e.g., tubing residence time affecting growth before SMPS sampling), this may indicate that a substantial fraction of ambient aerosol is a poor nucleation precursor (e.g., organic carbon), as suggested by regional composition measurements (Chou et al. 2010, 2022). It should also be noted that nucleation typically produces large numbers of freshly formed particles at sizes below 3 nm, whereas the lower detection limit of the SMPS is approximately 11 nm. Despite this limitation, our measured PSDs consistently show a sharp decrease in number concentration as they approach the 11 nm lower limit. One plausible explanation is the ~20 s residence time of the exhaust air in the sampling tubing, which allows newly nucleated particles to grow beyond the 11 nm limit.

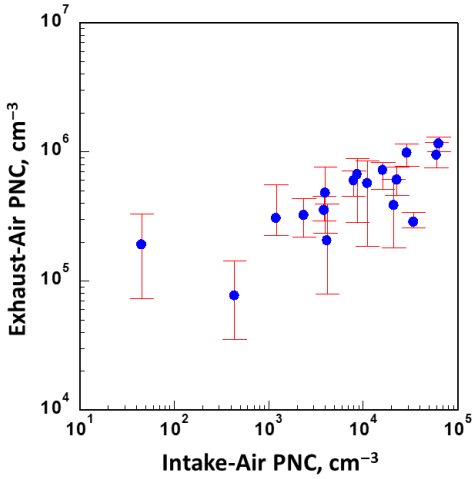

Figure 3: Exhaust PNC increases with intake aerosol loading.

3. Idealized Air Parcel Simulation

To interpret the laboratory results, we developed an aerosol parcel model (H_2SO_4–H_2O nucleation, condensation, coagulation) that resolves heating and cooling histories.

3.1 Model setup

The nucleation pathways for the RIN mechanism depends on the volatile compositions of aerosols, such as sulfate, nitrate, and organic compounds, which are all prevalent in the studied area. Under varying atmospheric conditions, aerosol nucleation proceeds mainly through the H_2SO_4–H_2O binary nucleation (Kulmala and Laaksonen 1990; Vehkamäki et al. 2002), ion-induced nucleation (Kusaka et al. 1995; Yu 2001), ternary and acid-base nucleation (Napari et al. 2002; Almeida et al. 2013, Dada et al. 2023), iodine-driven nucleation (O'Dowd et al. 2002, Wan et al. 2022), organic–dominated nucleation (Ehn et al. 2014; Kirkby et al. 2016). In this idealized modeling framework, we adopt the H_2SO_4–H_2O binary nucleation because it provides a well-established, internally consistent baseline. This choice allows us to isolate the direction and magnitude of the system response without introducing additional, poorly constrained parameters—particularly under extreme thermodynamic conditions such as those in combustion exhaust. Nucleation pathways such as NH_3- or organic-enhanced nucleation could amplify PNC production while not altering the qualitative direction of the sensitivities and responses reported here.

The parcel model used here is adapted from Chen et al. (2011), which employed a multi-component particle framework classifying aerosols by their water and sulfate mass. The model includes binary nucleation (H_2SO_4–H_2O), vapor condensation of both species (with solute/Raoult and curvature/Kelvin effects), and Brownian coagulation. The nucleation scheme follows

the classical binary nucleation theory, with an additional correction for the curvature dependence of surface tension (Chen et al. 2011). Conventional binary nucleation schemes tend to underestimate nucleation rates, whereas incorporating the curvature effect substantially improves performance, producing PNC values much closer to observations, as demonstrated by Chen et al. (2011). Each chemical component is discretized into 45 mass bins. For water, the bin range spans 1.0×10^{-24} to 1.0×10^{-9} mol; for sulfate, 1.0×10^{-24} to 5.6×10^{-11} mol. Changes in the particle spectrum along the mass coordinates—arising from condensation/evaporation and Brownian coagulation—are solved using a moment-conserving advection scheme that preserves both total mass and particle number across the discretized bins.

We simulated both in-cylinder heating and post-combustion cooling of an air parcel with idealized settings. For the heating phase, the parcel initially contains sulfate aerosol with geometric standard deviation (σ_g) and geometric mean diameter (D_g) prescribed from the urban aerosol PSD of Whitby (1978). Following typical engine transients (Heywood 2018), the temperature is ramped from 298 K to 800 K over 5 ms, representing rapid heating to the exhaust-header regime. It is then held at 800 K to assess particle survival under hot exhaust conditions. A temperature of 800 K corresponds approximately to the end-of-compression condition and therefore represents a lower bound of heating. In practice, simulations at temperatures above 800 K are largely unnecessary, however, because most particles are expected to fully evaporate at such elevated temperatures. The heating simulation uses a 0.1 ms time step throughout.

The cooling stage begins at T = 383 K (110 °C), below which the nucleation rate is negligible. Exhaust cooling is assumed to occur purely by conduction through the tailpipe, and we parameterize it with Newton's law of cooling using two measurements: an exhaust temperature of ~ 333 K at 15 cm downstream the tailpipe and a ~2 s travel time from cylinder to tailpipe exit. These constraints set the exponential cooling rate applied in the parcel model. The cooling simulation uses a 0.01 s time step. We further assume that a specified fraction of the seeded aerosol survives heating (i.e., does not fully evaporate). The residual particle sizes should decrease as they evaporate. However, the size spectrum of the residual particles depends not only on the initial loading but also on the duration and rate of evaporation, which are highly uncertain. To avoid introducing poorly constrained assumptions, we adopted a simplified approach in which the surviving particles retain the same chemical composition and PSD parameters (σ_g and D_g) as initially prescribed, but with a reduced number concentration. It should be noted that the simulations do not account for wall losses of vapors or particles, which are likely to occur in the laboratory experiments.

3.2 Simulation results

Figure 4a shows that, by the end of the combustion heating the PNC drops by nearly four orders of magnitude. Residual particles may remain, but they are negligible unless the initial aerosol loading is very high. At 800 K, most survivors persist for only a few milliseconds. The evaporation rate is regulated by aerosol loading: higher loadings release more H_2SO_4 (and/or SO_3) vapor, elevating its partial pressure and thereby slowing further evaporation. Consequently, more residual particles are expected at higher initial loadings, as seen in Fig. 4a. We note, however, that 800 K exceeds water's critical

temperature (647 K) and approaches the estimated critical temperature of sulfuric acid (~927 K), so the thermodynamic constraints are uncertain. To bracket this uncertainty, subsequent parcel simulations prescribe several evaporation fractions and assess the sensitivity of the residual-particle effect.

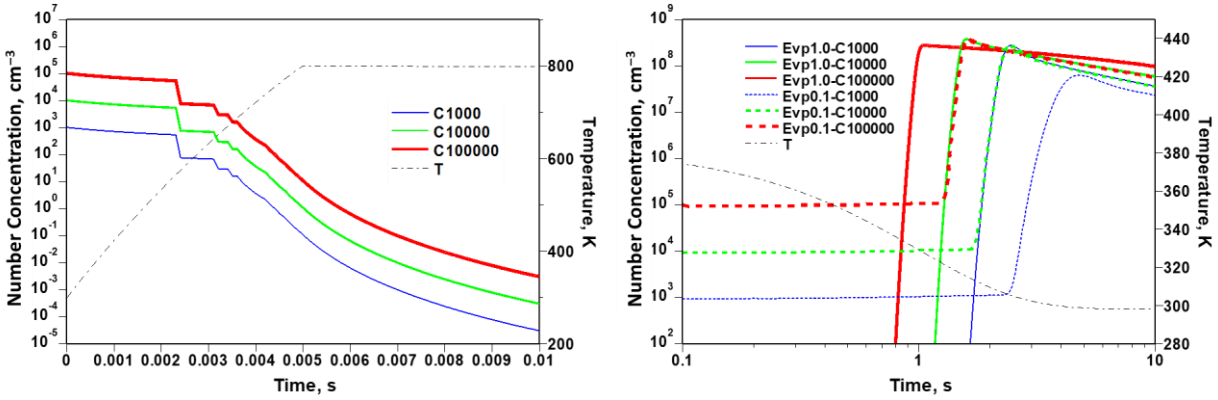

Figure 4: Simulated time evolution of particle concentration. (a) Heating: rapid evaporation; (b) Cooling: burst nucleation with sensitivity to the assumed evaporation fraction. Blue, green, and red curves correspond to initial aerosol number concentrations C= 10^3, 10^4, and 10^5 cm^{-3}, respectively. Solid and dashed lines denote 100% (Evp1.0) and 10% (Evp0.1) evaporation during the heating phase. The black dash–dot curve shows the parcel temperature (right-hand axis). The small zigzag pattern in panel (a) arises from numerical discretization of mass bins and is not a physical signal.

Figure 4b illustrates the time evolution of PNC during the cooling stage (for clarity, only the 100% and 10% evaporation cases are shown). As the parcel cools sufficiently, new particle formation is observed as a nucleation burst. This burst is directly triggered by the rapid increase in relative humidity (RH) and relative acidity (RA), defined as the ratio of H_2SO_4 vapor pressure to its saturation value, as detailed in Fig. 5. The burst initiated sooner when either the preexisting aerosol loading is higher or the evaporation fraction is larger, demonstrating its sensitivity to the availability of the H_2SO_4 vapor and RA. Following the onset, PNC rapidly rises to a peak and subsequently declines, a trend indicative of a self-limiting process: newly formed particles consume precursor vapors by condensation (which correlates with the rapid decrease of RA shown in Fig. 5), curbing further nucleation, and thereafter coagulation reduces particle number. For low evaporation fractions (e.g., 10%), the peak PNC increases with the input aerosol loading. Under 100% evaporation, however, the peak varies only weakly with loading; in fact, the peak is slightly higher for C= 10^4 cm^{-3} than for either 10^3 cm^{-3} or 10^5 cm^{-3}. This non-monotonic response further underscores the self-limiting nature of nucleation—especially at high initial loading and high evaporation fraction—where enhanced condensation and coagulation sinks dampen the growth of particle number despite abundant vapor.

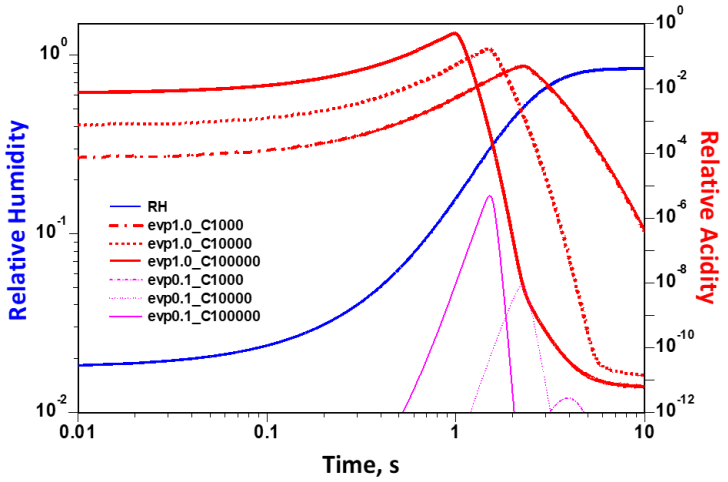

Figure 5: Time evolution of relative humidity (defined with respect to H_2O) and relative acidity (defined with respect to H_2SO_4 vapor) during the cooling stage (corresponding to the PNC evolution in Fig. 4b). Relative acidity (RA) is categorized by evaporation fraction (thick red curves: 100%; thin magenta curves: 10%) and by initial PNC (dash-dotted, dotted, and solid curves correspond to C= 10^3, 10^4, and 10^5 cm^{-3}, respectively). The initial mole fraction of H_2SO_4 vapor corresponding to C= 10^3, 10^4, and 10^5 cm^{-3} are $2.5x10^{-9}$, $2.5x10^{-8}$, and $2.5x10^{-7}$, respectively, assuming 100%. evaporation.

Figure 6 summarizes how the peak PNC varies with initial aerosol loading and evaporation fraction. Peak PNC increases sharply when both parameters are small, but the sensitivity progressively saturates at higher loadings and higher evaporation fractions, consistent with strengthening condensation/coagulation sinks. This saturation explains the relatively weak dependence of exhaust PNC on intake loading seen in Fig. 3, especially under high evaporation conditions. These results indicate that PNC production is highly responsive to changes in condensable vapor availability—modulated by intake/ambient aerosol loading and the particle vaporization fraction—and therefore to the effective nucleation rate. Importantly, these relationships reflect fundamental physical controls (competition between vapor generation/supersaturation and removal by condensation/coagulation sinks) that are expected to remain operative regardless of whether nucleation proceeds via binary, ternary, or organic-assisted pathways, even though the absolute nucleation efficiency may differ across mechanisms.

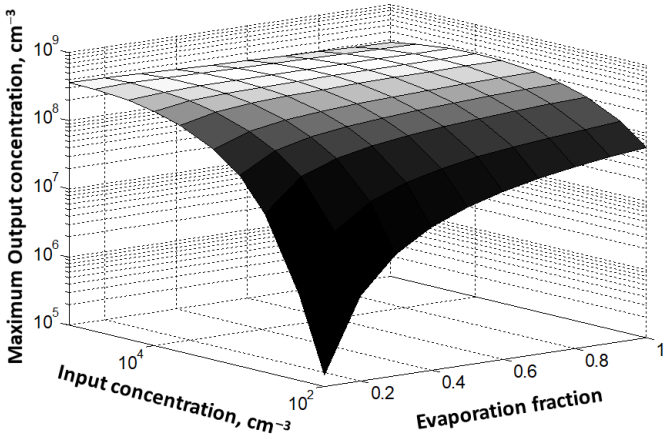

Figure 6: Peak PNC (applicate) produced by RIN from parcel simulations under varying input aerosol concentration (ordinate) and evaporation fraction (abscissa).

4. Regional Air Quality Simulations

We implemented a RIN parameterization in CMAQ and evaluated impacts on Aitken-mode PNC and $PM_{2.5}$. While the laboratory platform was a motorcycle, the proposed RIN mechanism is based on generic processes during combustion exhaust dilution and cooling —namely, vaporization of condensable material followed by nucleation/growth that are sensitive to background aerosol loading. These processes are not inherently unique to motorcycles. We therefore hypothesize RIN operates similarly across vehicle types, since peak burned-gas temperatures are broadly comparable and are sufficient to volatilize pre-existing aerosol particles. Accordingly, we apply the experimental results to both motorcycles and passenger cars in the model simulations. The mechanism is demonstrated and evaluated under Taiwan/West-Pacific urban conditions (high aerosol loading, suppressed regional NPF, and strong traffic influence over Taiwan, with observations at Xitun (Taichung).

4.1 Model setup

The Community Multiscale Air Quality (CMAQ) model, v4.7.1 (Byun and Schere 2006) was applied here for regional simulations. The gas–aerosol chemistry was augmented to include advanced aerosol processes—notably secondary organic aerosol formation and particle coagulation (Tsai et al. 2015a,b; Li et al. 2016a). Meteorological fields driving CMAQ were produced with the Weather Research and Forecasting (WRF) model, v3.7.1 (Skamarock et al. 2008). The modeling domains span East Asia (15°–36° N, 100°–140° E) to capture large-scale influences (East Asian monsoon, tropical cyclones) and major source regions. We employed two-way nesting with an outer domain at 10 km horizontal resolution and an inner

Taiwan domain at 2 km (Fig. 7). The vertical grid comprises 37 layers with enhanced resolution near the surface to better resolve turbulent mixing and vertical transport. Additional CMAQ and WRF configuration details are summarized in Table 1.

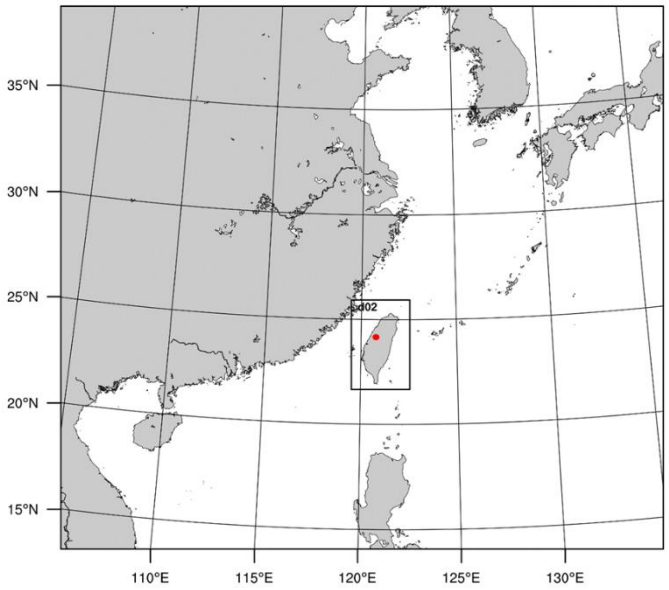

Figure 7: Map of CMAQ simulation domains. Xitun site marked.

Table 1: Model setup options for the CMAQ and WRF models.

Model	Modules
CMAQ	▪ Gas-phase chemistry mechanisms: SAPRC99 (Carter 2000) ▪ New particle formation mechanism: Kulmala et al. (1998) ▪ Anthropogenic emissions East Asia Emission Inventory: Multi-resolution Emission Inventory for China (MEIC), gridded at a 0.1° × 0.1° spatial resolution (http://meicmodel.org.cn) Taiwan Emission Inventory: Taiwan Emission Data System (TEDS) version 10, gridded at a 1 km × 1 km spatial resolution (https://air.moenv.gov.tw/airepaEn/EnvTopics/AirQuality_4.aspx) ▪ Biogenic emissions: Model of Emissions of Gases and Aerosols from Nature (MEGAN; Guenther et al. 2006), driven by MODIS land cover and leaf area index (LAI) datasets.
WRF	Initial and boundary conditions:

	ERA5 reanalysis data with a 0.25° × 0.25° horizontal resolution (Hersbach et al. 2016). Physics options: Goddard cloud microphysics scheme (Tao et al. 1989) Yonsei University planetary boundary layer scheme (Hong et al. 2006) RRTMG shortwave and longwave radiation schemes (Iacono et al. 2008) The unified Noah land surface model (Tewari et al. 2004) The Kain–Fritsch cumulus parameterization (Kain 2004), applied only to the outer domain

4.2 RIN mechanism setup

The RIN mechanism effectively converts ambient sulfate mass into new Aitken-mode particles. Based on the laboratory results presented in Section 3, the ambient sulfate mass contained in the intake air is assumed to evaporate completely under in-cylinder conditions. We estimate the conversion rate by the volume of ambient air processed by on-road engines—i.e., intake airflow multiplied by the ambient sulfate mass concentration. Intake airflow is linked to the fuel consumption rate via the air–fuel ratio (AFR). We assume a stoichiometric AFR = 14.7:1 (air:fuel by mass), typical of spark-ignition vehicles. The fuel consumption rate is inferred from the carbon emission rates (CO + CO_2) in the emission database using the stoichiometry of gasoline combustion (approximated as C_8H_{18}), following Heywood (2018). This approach yields a consistent, inventory-driven estimate of the ambient air volume processed—and thus the mass available for RIN-driven conversion into Aitken-mode number.

In addition to conserving the total mass of ambient aerosols, it is also necessary to define the PSD of newly formed particles to accurately simulate the effects of the RIN mechanism. In CMAQ, aerosol physical properties are represented using a tri-modal PSD that includes the Aitken, accumulation, and coarse modes. The nucleation mode discussed earlier is not explicitly distinguished from the Aitken mode in CMAQ. Each of the three modes is characterized by a log-normal distribution expressed as:

$$n(x) = \frac{N}{\sqrt{2\pi}\sigma} \exp\left[-\frac{1}{2}\left(\frac{x-\mu}{\sigma}\right)^2\right] \quad (1)$$

where $x = lnD$ is the natural logarithm of particle diameter (D), N is the PNC, $\mu = lnD_g$ is the modal value and $\sigma = ln\sigma_g$ is the standard deviation. The parameters D_g and σ_g are referred to as the geometric mean diameter and geometric standard deviation, respectively.

In CMAQ, the Aitken mode aerosol emission is assumed to have a D_g of 13 nm and σ_g of 1.7 for fine particles containing sulfate, nitrate, and elemental carbon (Elleman and Covert, 2010). The nucleation mode shown in Figure 2 from the Amb-In experiment can be approximated by a lognormal distribution with $D_g = 18$ nm and $\sigma_g = 1.16$. However, the particles observed in our measurements were likely hygroscopically grown, leading to significantly larger wet diameters than the dry particle sizes required for the CMAQ emission parameterization. In fact, the relative humidity of the exhaust air within the

buffer bag (cf. Fig. 1) was likely elevated, as condensation on the bag walls was frequently observed. Previous studies have demonstrated that the wet particle diameter can exceed the dry diameter by several times under relative humidity conditions greater than 90% (Chen 1994; Achtert et al. 2009; Zieger et al. 2017; Xu et al. 2024).

Here, we estimate the swelling ratio—defined as r_{eq}/r_d—using the diagnostic formula proposed by Chen et al. (2013) as follows:

$$r_{eq}/r_d = [1 + \kappa/(a_1 + a_2/RH + a_3/r_d)]^{1/3} \quad (2)$$

where r_{eq} denotes the equilibrium (wet) radius, r_d the dry radius, κ the hygroscopicity, and $a_1 = -1.02733$, $a_2 = 1.02654$, and $a_3 = 6.07891 \times 10^{-10}$ m are empirical fitting coefficients. The newly formed particles are likely composed primarily of water and sulfuric acid, which facilitate efficient binary nucleation. It is also possible that trace gases such as ammonia, volatilized from ambient aerosols, re-condense upon new particle formation. Accordingly, we estimate the swelling ratio by assuming the particles consist of either sulfuric acid or ammonium sulfate, adopting κ=1.19 for the former and κ=0.53 for the latter (Petters and Kreidenweis 2007). For a possible *RH* range of 90% to 100%, the swelling ratio r_{eq}/r_d derived from equation (2) for sulfuric acid particles ranges from 1.97 to 2.48, corresponding to D_g of 9.15 to 7.25 nm. For ammonium sulfate particles, the derived ratios are r_{eq}/r_d =1.61 to 2.06, yield D_g= 11.2 to 8.75 nm.

For our simulations, we selected D_g= 13 nm (the default CMAQ configuration) and D_g= 7.25 nm from the lower-bound of value range estimated above. The latter value represents conditions under high relative humidity. For σ_g, we adopted σ_g =1.7 (the default CMAQ setup) and σ_g =1.2 based on our experimental observation (rounded to the first digit). It should be note that σ_g of a dry spectrum may differ slightly from the that of the wet spectrum shown in Fig. 2, because the swelling ratio varies with particle sizes according to equation (2). However, accurately determining σ_g of the dry spectrum is challenging.

A control simulation (referred to as NoRIN) was performed with the RIN mechanism disabled to establish baseline comparisons. The combinations of D_g and σ_g values were used to design sensitivity experiments for evaluating the possible impact of the RIN mechanism on PNC (Table 2). The RIN_{CTRL} case represents the default CMAQ aerosol emission configuration, while RIN_D, RIN_σ, and $RIN_{D\sigma}$ denotes simulations with variations in the parameters D_g (denoted by subscript *D*) and σ_g (denoted by subscript σ). The NoRIN experiment thus serve as a reference case without the RIN mechanism.

Table 2: Comparison of mean $PM_{2.5}$ and PNC across experiments and observation. The values are average over the whole simulation period in November 2020.

	Geometric Standard Deviation	Modal Diameter (nm)	Average $PM_{2.5}$ ($\mu g\ m^{-3}$)	Average PNC (cm^{-3})
Observation			16.75	9354
NoRIN			20.31	2287
RIN_{CTRL}	1.7	13	20.66	2695
RIN_D	1.7	7.25	20.29	4174
RIN_σ	1.2	13	20.26	3361
$RIN_{D\sigma}$	1.2	7.25	20.41	7307

4.3 Aerosol measurement data

For verification of PNC in the simulation results, we utilized hourly PSD data measured during a non-operational mission at the Xitun air quality monitoring station (24°09′41.4″ N, 120°37′02.6″ E), conducted by the Ministry of Environment. The Xitun station is located near the center of Taichung City, the second-largest metropolitan area in Taiwan. The instruments used for PNC measurement included a GRIMM Scanning Mobility Particle Sizer (SMPS+C; GRIMM Aerosol Technik Ainring GmbH & Co. KG, Germany), which measures particle diameters ranging from 5 to 350 nm across 117 size channels, and a GRIMM Environmental Dust Monitor (EDM 180), which covers the 0.25–32 μm size range with 31 channels. In addition, hourly $PM_{2.5}$ mass concentrations routinely obtained from a Beta Attenuation Mass Monitor (BAM 1020; Met One Instruments Inc.) at the Xitun station were also analyzed for comparison.

Considering the availability of PNC measurements, simulations were conducted for the period of November 5–25, 2020. During this period, a total of 54 hours of PNC data were missing—primarily on November 15–16—and only 5 hours of $PM_{2.5}$ data were unavailable. These data gaps were excluded from the subsequent analyses.

4.4 Simulations results

On average, the NoRIN run overestimated $PM_{2.5}$ by 21% while underestimated PNC by 75% (Table 2). Introducing the RIN mechanism had little effect on $PM_{2.5}$ but substantially improved PNC, reducing the underestimation to 71% in RIN_{CTRL}. The results were sensitive to the assumed PSD parameters. With D_g=7.25 nm (RIN_D), the PNC bias reduced to 55%; with $\sigma_g = 1.2$ (RIN_σ), it decreased to 64%. Replacing both parameters simultaneously ($RIN_{D\sigma}$) further reduced the PNC underestimation to 22%. Comparisons of simulated and observed PNC for this period are shown in Fig. S5.

The opposing biases in PNC and $PM_{2.5}$ suggest the presence of a missing process that influences particle number and mass differently. This discrepancy likely precludes emission inventory error or meteorological uncertainties—such as inaccurate advection or turbulent mixing—as the primary drivers of the PNC shortfall, as these factors would typically exert a monotonic influence on both metrics. Conversely, the RIN mechanism is intrinsically mass-neutral, while significantly enhances PNC, thereby reproducing the observed bias pattern.

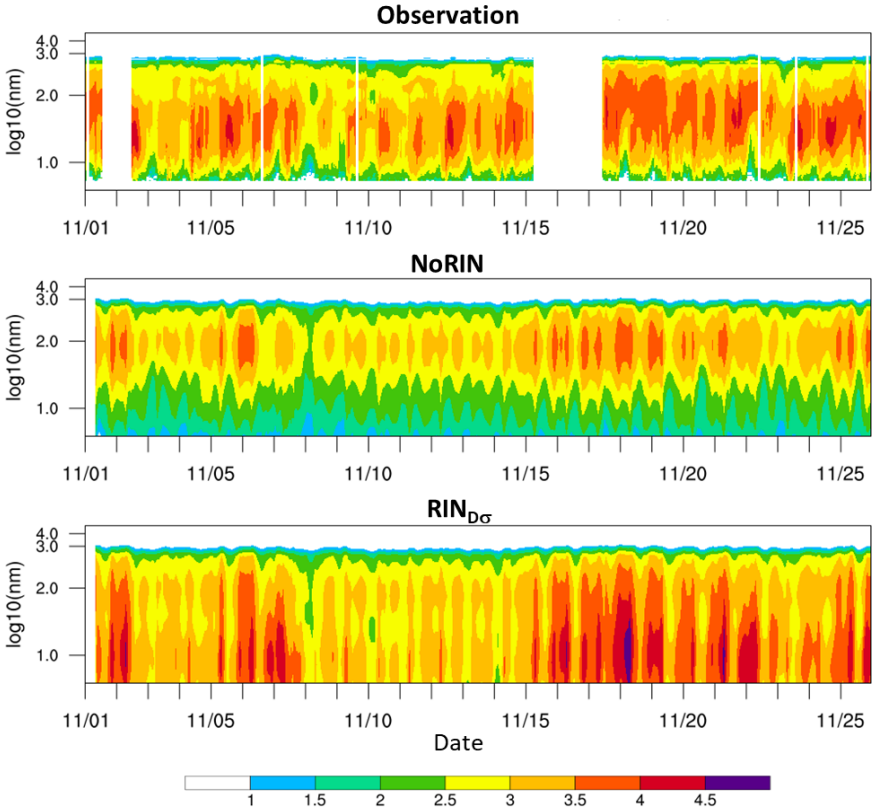

Figure 8. Time evolution of the particle number size distribution (dN/dlogD) at Xitun during November 2020. Panels (top to bottom) show the observation, the NoRIN simulation, and the $RIN_{D\sigma}$ simulation. The ordinate shows particle diameter (nm), and the abscissa shows dates in November 2020. The color bar indicates number density (dN/dlogD; cm^{-3}) on a base-10 logarithmic scale, with null values masked. Results for RIN_D and RIN_σ scenarios are not shown for brevity.

Figure 8 compares simulated and observed PSD over the full simulation period for the two end-member cases, NoRIN and $RIN_{D\sigma}$. The NoRIN simulation markedly underestimates PNC, with the largest biases at the smallest diameters. Including RIN ($RIN_{D\sigma}$) substantially enhances ultrafine particle numbers and substantially restores the Aitken-mode population. However, the smallest size bins remain somewhat over-enhanced, even though the total PNC is still slightly lower than observed. Other RIN scenarios (not shown for brevity) yield a weaker Aitken-mode tail, but at the expense of a larger underestimation in total PNC.

One plausible explanation is that the simulated Aitken-mode PSD becomes overly broad, which inflates the distribution tails—most notably the sub-10 nm number concentration. The mean Aitken-model σ_g derived from the $RIN_{D\sigma}$ simulation is 2.47, substantially higher than the $\sigma_g = 2.14$ obtained by fitting the observed Aitken-mode PSD. Notably, CMAQ enforces an upper bound of $\sigma_g = 2.5$; thus, the true degree of broadening could be even larger if this constraint were relaxed. Such bias reflects not only uncertainties in early-growth processes (e.g., condensation and coagulation), but also limitations inherent to the modal representation in CMAQ. In the current framework, newly formed particles are not represented as a distinct, externally mixed population. Instead, they are immediately assimilated into the pre-existing Aitken mode, which already includes ambient and primary-emitted particles characterized by larger modal diameters and broader geometric standard deviations. This artificial assimilation inevitably broadens the simulated Aitken-mode size distribution and inflates the small-diameter tail. In reality, freshly nucleated particles would initially remain as a separate nucleation-mode population and would be removed efficiently through self-coagulation and scavenging by pre-existing Aitken-mode particles. As a result, far fewer particles would persist in the sub-10 nm range, and the nucleation-mode signature would be less pronounced than implied by the merged-mode treatment.

A related issue is mixing state. Physically, freshly nucleated particles should initially remain largely externally mixed and can exhibit composition-dependent growth rates. In CMAQ, however, they are treated as internally mixed within the host mode, which can alter condensational growth and coagulation dynamics relative to an externally mixed treatment. A rigorous separation of the contributions from (i) growth-process parameterization, (ii) modal merging/broadening, and (iii) mixing-state assumptions would require additional model development and sensitivity experiments that are beyond the scope of this study.

In addition to the period-wide evaluation in Table 2 and Figure 8, we further examined the hourly evolution of aerosol properties by zooming in on two representative days (November 20 and 25). Because the RIN mechanism is closely linked to traffic activity and its pronounced diurnal cycle, these two days were selected to illustrate RIN-related temporal dynamics. Both days were characterized by fair weather conditions under mild northeasterly monsoon flow (cf. Figs. S2 and S3), providing stable regional background conditions suitable for evaluating RIN-related variations. As shown in Figs. 9a and 9b, the simulated $PM_{2.5}$ concentrations were approximately twice the observed values during the early morning hours, likely due to a low bias in the nighttime planetary boundary layer height (PBLH). This bias is a well-documented issue in CMAQ simulations (e.g., Du et al. 2020; Cheng et al. 2021; Chuang et al. 2023) and is more pronounced on November 25. In contrast, $PM_{2.5}$ tends to be underestimated from late afternoon through evening. The morning $PM_{2.5}$ peak associated with rush-hour traffic is clearly reproduced, although the timing of the peak may be slightly shifted. However, the nighttime peaks observed in the measurements are not evident in the simulations for either day, likely reflecting deficiencies in simulating the timing and intensity of land-breeze development. In addition, the discrepancies may also arise from inaccuracies in the emission inventory, particularly regarding the diurnal emission profiles (Tsai et al. 2021; Chen et al. 2024). These modeling limitations, however, are beyond the scope of the present study and are not further discussed here.

The contrasting biases in $PM_{2.5}$ and PNC observed in the monthly averages (Table 2) become even more apparent on the

selected analysis days. As shown in Figs. 9c and 9d, the NoRIN simulation produced substantially underestimated PNC values, despite exhibiting a positive bias in $PM_{2.5}$. The simulated morning PNC peak was less than one-quarter of the observed value, and the discrepancy was even greater during the evening hours on both days. Incorporating the RIN mechanism led to notable improvements in PNC performance. For example, RIN_{CTRL} increased the morning peak PNC by approximately one-third, while RIN_{σ} doubled this improvement and RIN_{D} tripled it, resulting in a peak magnitude approaching the observed value.

When both parameters—D_g and σ_g—were replaced with those derived from our experimental measurements ($RIN_{D\sigma}$), the morning peak PNC appeared overestimated. However, considering that the simulated $PM_{2.5}$ peak was approximately twice the observed value, and that RIN-induced PNC production scales with ambient $PM_{2.5}$, the $RIN_{D\sigma}$ results remain physically consistent. Moreover, in the $RIN_{D\sigma}$ case, the behaviors of $PM_{2.5}$ and PNC were mutually consistent—both were overestimated in the morning and slightly underestimated in the evening. In contrast, other RIN configurations continued to produce low PNC values despite the morning overestimation of $PM_{2.5}$, underscoring the sensitivity of the RIN mechanism to PSD parameters.

It is important to note that new particle production via the RIN mechanism is closely linked to traffic activity. Consequently, even though $PM_{2.5}$ concentrations are elevated during the early morning hours—particularly on November 25—the PNC remains low until approximately 4–5 a.m., when traffic emissions begin to increase.

Notably, the modeled PNC peak precedes the $PM_{2.5}$ peak, a behavior consistent with observational findings reported by Chen (1999). Moreover, the rapid decline in simulated PNC also occurs earlier than that of $PM_{2.5}$, which is likely attributable to self-limiting effects associated with the coagulation sink, as discussed previously.

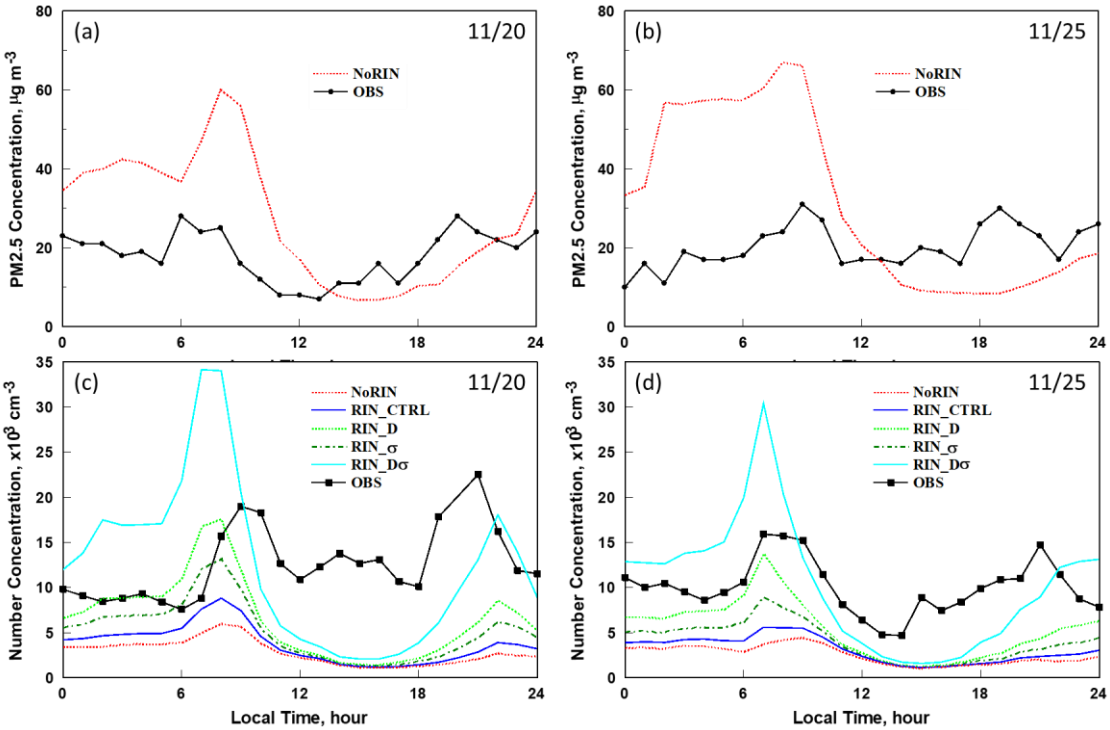

Figure 9: Comparison of simulated and observed hourly variations of $PM_{2.5}$ (top) and PNC (bottom) on the two selected days. The simulated $PM_{2.5}$ values are from the RIN_{CTRL} experiment, as results from other RIN cases are nearly identical. Observed values (OBS) are shown as black solid lines, while simulations from NoRIN, RIN_{CTRL}, RIN_D, RIN_σ, and $RIN_{D\sigma}$ are represented by red dotted, blue solid, light green dotted, dark green dash-dotted, and cyan solid lines, respectively.

Figure 10 presents the simulated spatial distribution of PNC over Taiwan, averaged for November 20, 2020. A pronounced contrast is evident between the NoRIN and $RIN_{D\sigma}$ scenarios, particularly in the partitioning between the Aitken and accumulation modes. In the absence of the RIN mechanism, aerosol particles are predominantly concentrated in the accumulation mode. In contrast, when the RIN mechanism is included, Aitken-mode particles dominate the total PNC. The PSD measurements at Xitun on the same day (see Supplement Fig. S6) support the $RIN_{D\sigma}$ results, showing that the Aitken mode particles (<100 nm) were approximately two to five times more abundant than those in the accumulation mode (100 nm–1 μm), with a mean ratio of 3.4. On November 25, this ratio increased to 5.7 (ranging from approximately three to seven). The $RIN_{D\sigma}$ simulation produced a comparable Aitken-to-accumulation ratio of about four to five, demonstrating reasonable agreement with the observations.

Figure 10 also illustrates that the RIN mechanism generally reduces accumulation-mode PNC, though the absolute magnitude of this decrease is modest. This limited reduction is likely due to replenishment through condensational growth and coagulation of newly formed particles. The spatial patterns for November 25, as well as those from other RIN simulations (RIN_{CTRL}, RIN_D, and RIN_σ) are qualitatively similar and therefore not shown here (see supplement Fig. S7).

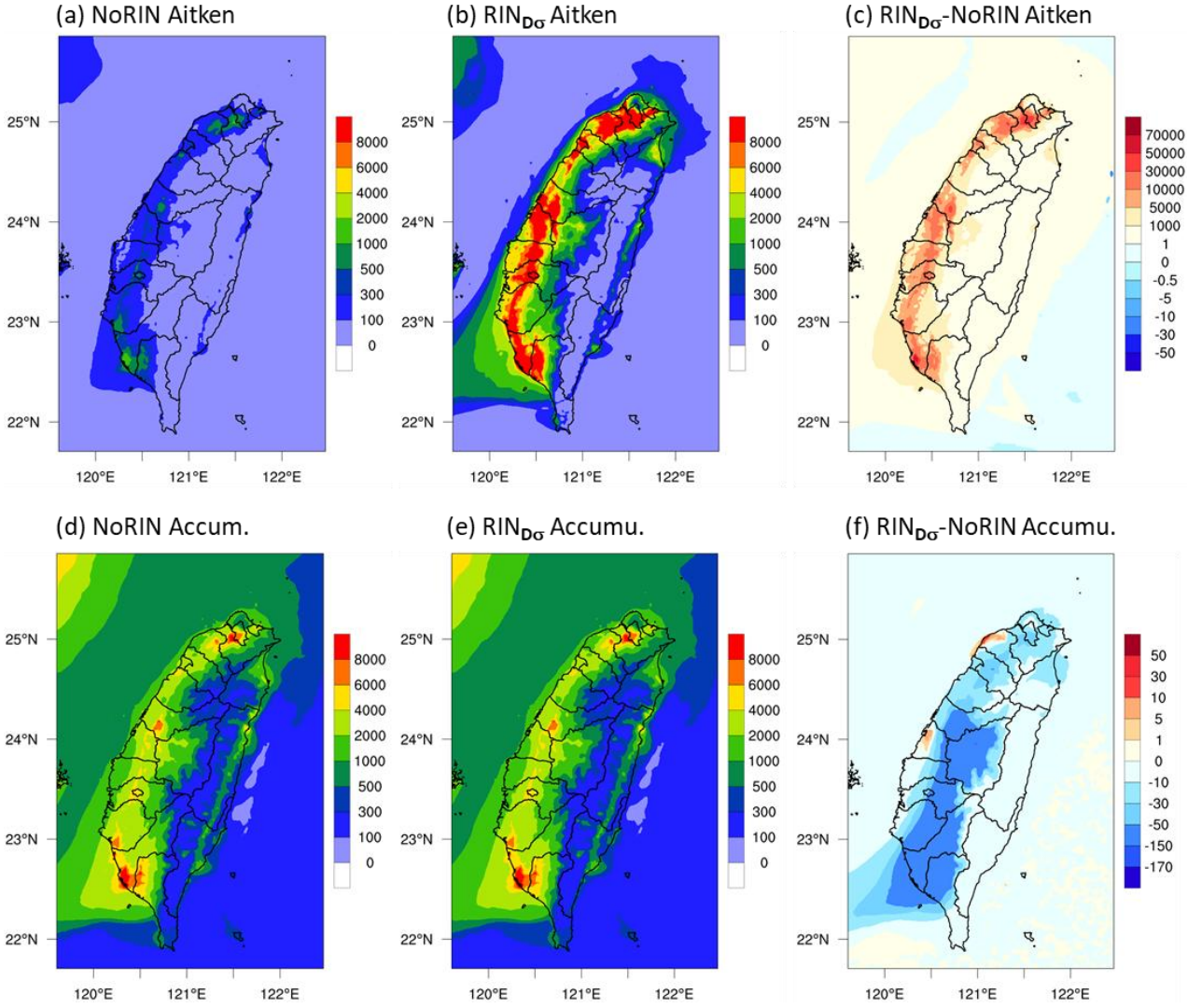

Figure 10: Daily Aitken- and Accumulation-mode PNC (in cm^{-3}) from the November 20 simulation. Panels (a)–(c) show results from the NoRIN, RIN$_{D\sigma}$, and RIN$_{D\sigma}$–NoRIN cases, respectively. For visual consistency, an upper limit of 10,000 cm^{-3} is applied to the color scale in the PNC plots. However, the Aitken-mode PNC in the RIN$_{D\sigma}$ simulation (panel b) frequently exceeds this limit. Panel (c) therefore provides a clearer depiction of regions with elevated PNC concentrations.

5. Discussion and Conclusion

5.1 Mechanistic insights and model implications

This study provides laboratory and modeling evidence supporting RIN as a physically plausible and atmospherically relevant pathway for new particle formation in urban environment. Laboratory experiments demonstrated that nucleation-mode

particles emerge only when ambient aerosols are present in the intake air, confirming that pre-existing aerosols can undergo in-cylinder vaporization and subsequent re-nucleation during exhaust cooling. This process effectively converts accumulation-mode mass into Aitken-mode number, consistent with the observed PSD shifts in both engine exhaust and regional simulations.

Parcel-model simulations further elucidated the underlying microphysics of RIN. The results reveal a self-limiting nucleation process, whereby rapid particle formation enhances condensation and coagulation sinks that suppress further number growth. The sensitivity of peak PNC to both aerosol loading and evaporation fraction exhibited a saturation behavior, explaining why exhaust PNC increases sub-linearly with intake aerosol abundance in the laboratory. These findings underscore that RIN represents a secondary transformation process constrained by thermodynamic and microphysical feedbacks, rather than a simple linear source of ultrafine particles.

5.2 Urban-scale effects and model evaluation

When implemented in the CMAQ regional air-quality model, demonstrated and evaluated under Taiwan/West-Pacific urban conditions, the RIN mechanism substantially reduces low bias in Aitken-mode PNC while maintaining $PM_{2.5}$ mass consistency. Without RIN, the model exhibited a 75% underestimation of PNC and a 21% overestimation of $PM_{2.5}$. The opposite biases in PNC and PM2.5 are likely a common behavior of current air-quality models. Including RIN reduced the PNC bias down to 14% in the most physically consistent configuration ($RIN_{D\sigma}$), while the $PM_{2.5}$ bias remained largely unchanged. This contrasting response highlights the decoupled behavior of mass and number, supporting the hypothesis that traditional models omit a key mechanism influencing PNC in urban environments.

The diurnal analyses revealed that RIN-driven PNC peaks coincide with morning traffic activity, while $PM_{2.5}$ peaks occur later, reflecting the time lag between number production and mass accumulation. The earlier rise and faster decay of simulated PNC relative to $PM_{2.5}$ are consistent with both observational patterns (Chen 1999) and the coagulation-sink self-limitation seen in parcel modeling. This temporal behavior confirms that RIN is directly tied to vehicle emissions and acts on short timescales, making it a critical process for urban ultrafine particle dynamics.

Spatially, the inclusion of RIN markedly increased Aitken-mode PNC over major traffic corridors and metropolitan centers while slightly reducing accumulation-mode concentrations. The modeled Aitken-to-accumulation ratio (4–5) matched observations at the Xitun site, reinforcing the physical realism of the parameterization. Without the RIN mechanism, the ratio falls far below unity. The limited impact on accumulation-mode particles reflects compensating processes: while some mass is transferred to smaller sizes via re-nucleation, condensational growth and coagulation partially restore the accumulation population, maintaining overall mass balance.

5.3 Implications for air quality and health assessment

The findings carry important implications for both air quality modeling and public health assessment. Conventional emission inventories and model frameworks emphasize mass-based metrics ($PM_{2.5}$), yet this study demonstrates that such approaches

can miss major number-based processes. The RIN mechanism provides a mechanistic explanation for the long-standing low-PNC bias seen in regional simulations. Incorporating RIN thus enhances the predictive capability of urban-scale PNC, a parameter more directly linked to ultrafine particle exposure and associated health effects.

Furthermore, because RIN depends on ambient aerosol composition and humidity, it may vary across different climatic and emission regimes. Regions with high sulfate and ammonium contents—such as East and Southeast Asia—are particularly conducive to RIN due to the high volatility of these compounds at combustion temperatures and their strong hygroscopic properties upon cooling. Consequently, including RIN in emission and chemical transport models could be critical for accurate exposure assessments in densely populated areas with intense traffic emissions.

5.4 Limitations and future directions

Although the experimental and modeling results collectively support RIN as a key urban aerosol process, several uncertainties remain. The current laboratory setup used a single-engine configuration under steady operating conditions; thus, future studies should extend testing to diverse engine types, fuels, and transient driving cycles. More comprehensive chemical and optical characterizations (e.g., SP2 for black carbon, PTR-ToF-MS for condensable organics) are also needed to refine the composition and volatility assumptions underlying the RIN parameterization.

In principle, the RIN mechanism applies to any combustion process that ingests ambient air containing pre-existing aerosols. Its relative importance, however, is modulated by the competition with other nucleation pathways driven by fuel-derived combustion products. In most developed regions, such as the European Union and Taiwan, ultra-low sulfur standards (e.g., ≤10 ppm by mass) have converged the sulfur content of on-road diesel and gasoline. Under these regulated conditions, the magnitude of fuel-sulfur-driven nucleation is expected to be comparable across both engine types, suggesting that the RIN mechanism operates with similar significance in both cases. Conversely, fuels used in marine shipping and certain aviation applications may contain sulfur concentrations of several thousand ppm, triggering potent sulfuric-acid-driven nucleation during exhaust cooling. In such high-sulfur scenarios, fuel-derived sulfate production may equal or exceed the particle formation associated with RIN, requiring both sources to be considered jointly. These high-emission sources, however, fall outside the scope of the present study, which focuses specifically on urban environments dominated by on-road traffic.

Nucleation involving volatile organic compounds (VOCs) represents another potential pathway. While sulfuric acid has traditionally been regarded as the primary driver of new particle formation, recent research has demonstrated that highly oxygenated organic molecules can be significant, or even dominant, contributors in certain environments. Nevertheless, our purified-air experiments indicate that particle production from fuel-only combustion—including VOC emissions from gasoline—is substantially weaker than that associated with the RIN mechanism under our experimental conditions. We emphasize, however, that this conclusion is currently limited to gasoline-engine experiments. The potential significance of VOC-induced nucleation in diesel engines or other combustion sources remains uncertain and warrants further investigation with laboratory or modeling studies.

We acknowledge, however, that vehicle type, engine technology, and operating conditions (e.g., engine load, exhaust after-

treatment, and cooling rates) can influence the quantitative strength of RIN by modifying factors such as evaporation efficiency, exhaust cooling timescales, and interactions with combustion residues. These factors may affect the magnitude of particle number production but are not expected to suppress the underlying mechanism itself. Accordingly, we interpret the parameterization developed in this study as representing the order-of-magnitude impact and qualitative behavior of RIN under typical urban driving conditions, rather than a vehicle-specific emission factor. We hypothesize that the RIN mechanism may be applicable to other combustion sources and regions, but this potential transferability remains to be tested with additional measurements and targeted evaluations.

In the modeling domain, the parameterization currently assumes uniform mixing of ambient aerosols and exhaust flows and instantaneous vaporization, which may not fully capture plume-scale and microscale interactions near emission sources. Further coupling of RIN with real-time traffic emission models, sub-grid plume dispersion, and aerosol microphysics modules could improve representation of near-road environments. Finally, long-term monitoring of size-resolved number concentrations in multiple cities will be essential to evaluate RIN's regional significance and its potential contribution to ultrafine particle exposure risk.

An additional limitation is the overestimation of particle number concentrations in the smallest size range when the RIN mechanism is included. Although the Aitken-mode number concentrations remain reasonable—and in some cases still slightly underestimated in the monthly averages—the model overpredicts particle numbers at the lower end of the size distribution (Fig. 8). This reflects not only enhanced particle production by RIN, but also limitations in the PSD representation. Analysis indicates that σ_g of the simulated Aitken mode is systematically broader than observed, even with the upper bound imposed in CMAQ. This bias exists in the baseline simulation and is amplified by RIN, leading to artificial spreading of particle number into the smallest size bins. Consequently, part of the apparent improvement in total particle number arises from redistribution within the PSD rather than an accurate size-resolved representation. In addition, uncertainties in the parameterization of RIN-generated particles (e.g., assumptions for D_g and σ_g) may further contribute to this size-dependent discrepancy.

This σ_g-related bias is consistent with known limitations of modal aerosol schemes, in which a limited number of lognormal modes with prescribed or weakly constrained σ_g can introduce structural biases (Binkowski and Roselle, 2003; Elleman and Covert, 2010). Modal approaches tend to artificially broaden size distributions—particularly in the ultrafine range—due to their inability to explicitly resolve distinct nucleation modes (Mann et al., 2012), and similar PSD-related biases have been reported in regional models (Sartelet et al., 2022). These findings indicate that the impact of RIN is strongly conditioned by the underlying PSD framework. In the current modal structure, newly formed particles are immediately merged into the Aitken mode, precluding representation of a distinct nucleation mode. Addressing this limitation would require improved PSD treatments (e.g., inclusion of an explicit nucleation mode or adoption of sectional approaches) and refinement of early growth parameterizations; however, such developments would involve substantial restructuring of the aerosol representation and are therefore beyond the scope of the present study.

5.5 Conclusions

This study establishes a comprehensive, multi-scale framework linking laboratory observations, parcel modeling, and regional simulations to demonstrate the atmospheric relevance of RIN. The key findings are summarized as follows:

- Laboratory evidence confirms that RIN occurs only when ambient aerosols are present in engine intake air, producing a strong nucleation mode while depleting accumulation particles.
- Parcel-model simulations reveal that RIN-driven nucleation is self-limiting, with condensation and coagulation sinks governing the peak PNC response.
- Regional CMAQ simulations incorporating RIN significantly improve PNC predictions in Taichung, reducing underestimation from 75% to 22%, while maintaining realistic $PM_{2.5}$ levels.
- RIN offers a physically grounded explanation for the commonly observed low-PNC/high-$PM_{2.5}$ bias in air-quality models.
- The mechanism's sensitivity to ambient composition, humidity, and traffic activity highlights its importance for urban-scale particle dynamics and health-relevant air-quality assessments.
- Overall, RIN provides a missing link between combustion microphysics and ambient PNC. Incorporating this process into air-quality modeling frameworks represents a critical step toward more accurate predictions of ultrafine particle exposure, advancing both scientific understanding and public health protection.

Data and availability

The PSD measurements and key simulation outputs from this study are available via a GitHub repository at https://doi.org/10.5281/zenodo.20003687.

Code availability

The CMAQ-RIN module developed in this study is available from the corresponding author upon reasonable request.

Author contribution

J.-P. Chen conceived and supervised the study.

G.-D. Hwang and L.-W. Kuo designed and conducted the laboratory engine experiments.

J.-P. Chen developed the parcel-model simulations and L.-W. Kuo analyzed the simulation results.

I-C. Tsai implemented and performed the CMAQ model simulations.

J.-P. Chen and I-C. Tsai processed and analyzed the observational particle size distribution data.

J.-P. Chen interpreted the results and synthesized the findings.

J.-P. Chen wrote the manuscript with contributions from all co-authors.

All authors reviewed and approved the final version of the paper.

Competing interests

The authors declare no competing financial or personal interests that could have influenced the work reported in this study.

Acknowledgements

This study was supported through Grants NSTC 111-2811-M-002-077-MY3 and NSTC 113-2111-M-002-002.

Reference

Achtert, P., Birmili, W., Nowak, A., Wehner, B., Wiedensohler, A., Takegawa, N., … Zhu, T.: Hygroscopic growth of tropospheric particle number size distributions over the North China Plain, J. Geophys. Res. Atmos., 114, D00G07, https://doi.org/10.1029/2008JD010921, 2009.

Albritton, D. and Greenbaum, D. S.: Atmospheric observations: Helping build the scientific basis for decisions related to airborne particulate matter, in: PM Measurements Research Workshop, Health Effects Institute, Chapel Hill, NC, 9–12, 1998.

Almeida, J., Schobesberger, S., Kürten, A. et al.: Molecular understanding of sulphuric acid–amine particle nucleation in the atmosphere. Nature 502, 359–363, https://doi.org/10.1038/nature12663, 2013

Balmes, J. R. and Hansel, N. N.: Tiny particles, big health impacts, Am. J. Respir. Crit. Care Med., 210, 1291–1292, https://doi.org/10.1164/rccm.202407-1476ED, 2024.

Binkowski, F. S. and Roselle, S. J.: Models-3 Community Multiscale Air Quality (CMAQ) model aerosol component: 1. Model description, J. Geophys. Res., 108(D6), 4183, https://doi.org/10.1029/2001JD001409, 2003.

Byun, D. and Schere, K. L.: Review of the governing equations, computational algorithms, and other components of the Models-3 Community Multiscale Air Quality (CMAQ) modeling system, Appl. Mech. Rev., 59, 51, https://doi.org/10.1115/1.2128636, 2006.

Carter, W. P. L.: Documentation of the SAPRC-99 chemical mechanism for VOC reactivity assessment, Final Report to CARB, 95–308, available at: https://api.semanticscholar.org/CorpusID:92723073 (last access: October 1, 2025), 2000.

Chen, J.-P.: Theory of deliquescence and modified Köhler curves. J. Atmos. Sci., 51, 3505–3516, https://doi.org/10.1175/1520-0469(1994)051%3C3505:TODAMK%3E2.0.CO;2, 1994.

Chen, J.-P.: Particle nucleation by recondensation in combustion exhausts, Geophys. Res. Lett., 26, 2403–2406, https://doi.org/10.1029/1999GL900510, 1999.

Chen, J.-P., Tsai, T.-S., and Liu, S.-C.: Aerosol nucleation spikes in the planetary boundary layer, Atmos. Chem. Phys., 11, 7171–7184, https://doi.org/10.5194/acp-11-7171-2011, 2011.

Chen, J.-P., Tsai, I.-C., and Lin, Y.-C.: A statistical–numerical aerosol parameterization scheme, Atmos. Chem. Phys., 13, 10483–10504, https://doi.org/10.5194/acp-13-10483-2013, 2013.

Chen, L., Zhang, F., Zhang, D., Wang, X., Song, W., Liu, J., … Li, Z.: Hygroscopic growth of ambient fine particles

measured at five sites in China, Atmos. Chem. Phys., 22, 6773–6786, https://doi.org/ 10.5194/acp-22-6773-2022, 2022.

Chen, X., Yu, F., Yang, W., Sun, Y., Chen, H., Du, W., … Wang, Z.: Global–regional nested simulation of particle number concentration by combining microphysical processes with an evolving organic aerosol module, Atmos. Chem. Phys., 21, 9343–9366, https://doi.org/10.5194/acp-21-9343-2021, 2021.

Chen, Y.-W., Liu, K.-T., Thao, H. T. P., Jian, M.-Y., and Cheng, Y.-H.: Insight into the diurnal variations and potential sources of ambient $PM_{2.5}$-bound polycyclic aromatic hydrocarbons during spring in Northern Taiwan, J. Hazard. Mater., 476, 134977, https://doi.org/ 10.1016/j.jhazmat.2024.134977, 2024.

Cheng, F.-Y., Feng, C.-Y., Yang, Z.-M., Hsu, C.-H., Chan, K.-W., Lee, C.-Y., and Chang, S.-C.: Evaluation of real-time $PM_{2.5}$ forecasts with the WRF–CMAQ modeling system and weather-pattern-dependent bias-adjusted $PM_{2.5}$ forecasts in Taiwan, Atmos. Environ., 244, 117909, https://doi.org/ 10.1016/j.atmosenv.2020.117909, 2021.

Chou, C. C.-K., Lee, C.-T., Cheng, M.-T., Yuan, C.-S., Chen, S.-J., Wu, Y.-L., … Liu, S.-C.: Seasonal variation and spatial distribution of carbonaceous aerosols in Taiwan, Atmos. Chem. Phys., 10, 9563–9578, https://doi.org/ 10.5194/acp-10-9563-2010, 2010.

Chou, C. C.-K., Lung, S.-C. C., Hsiao, T.-C., and Lee, C.-T.: Regional and urban air quality in East Asia: Taiwan, in: Handbook of Air Quality and Climate Change, Springer, Singapore, https://doi.org/ 10.1007/978-981-15-2527-8_71-1, 2022.

Chuang, M.-T., Chou, C. C.-K., Lin, C.-Y., Lee, J.-H., Lin, W.-C., Chen, W.-N., … Chang, C.-C.: Probing air pollution in the Taichung metropolitan area, Taiwan. Part 1: Comprehensive model evaluation and the spatio-temporal evolution of a $PM_{2.5}$ pollution event, Atmos. Res., 287, 106713, https://doi.org/ 10.1016/j.atmosres.2023.106713, 2023.

Chung, M., Wang, D. D., Rizzo, A. M., Gachette, D., Delnord, M., Parambi, R., … Brugge, D.: Association of PNC, BC, and $PM_{2.5}$ with blood pressure in a near-highway population, Int. J. Environ. Res. Public Health, 12, 2765–2780, https://doi.org/10.3390/ijerph120302765, 2015.

Dada, L., Okuljar, M., Shen, J., et al.: The synergistic role of sulfuric acid, ammonia and organics in particle formation over an agricultural land. Environmental science: atmospheres, 3(8), 1195-1211, https://doi.org/10.1039/D3EA00065F, 2023.

Dal Maso, M. I. I. K. K. A., Kulmala, M., Lehtinen, K. E., Mäkelä, J. M., Aalto, P., and O'Dowd, C. D.: Condensation and coagulation sinks and formation of nucleation mode particles in coastal and boreal forest boundary layers. Journal of Geophysical Research: Atmospheres, 107(D19), PAR-2, https://doi.org/10.1029/2001JD001053, 2002.

Du, Q., Zhao, C., Zhang, M., Dong, X., et al.: Modeling diurnal variation of surface $PM_{2.5}$ over East China with WRF-Chem: impacts from boundary-layer mixing and anthropogenic emission, Atmos. Chem. Phys., 20, 2839–2863, https://doi.org/ 10.5194/acp-20-2839-2020, 2020.

Dunne, E. M., Gordon, H., Kürten, A., Almeida, J., Duplissy, J., Williamson, C., … Carslaw, K. S.: Global atmospheric particle formation from CERN CLOUD measurements, Science, 354, 1119–1124, https://doi.org/ 10.1126/science.aaf2649, 2016.

Elleman, R. A. and Covert, D. S.: Aerosol size distribution modeling with CMAQ: 3. Size distribution of emitted particles, J. Geophys. Res. Atmos., 115, D03207, https://doi.org/ 10.1029/2009JD012401, 2010.

Fanourgakis, G. S., Kanakidou, M., Nenes, A., Bauer, S. E., Bergman, T., Carslaw, K. S., … Yu, F.: Evaluation of global simulations of aerosol particle number and CCN number, Atmos. Chem. Phys., 19, 8591–8617, https://doi.org/ 10.5194/acp-19-8591-2019, 2019.

Fleig, D., Alzueta, M. U., Normann, F., Abián, M., Andersson, K., and Johnsson, F.: Formation of SO_3 under post-flame conditions: experiments and modeling, Combust. Flame, 160, 1142–1151, https://doi.org/ 10.1016/j.combustflame.2013.02.002, 2013.

Gani, S., Bhandari, S., Patel, K., Seraj, S., Soni, P., Arub, Z., Habib, G., Hildebrandt Ruiz, L., and Apte, J. S.: Particle number concentrations and size distribution in a polluted megacity: the Delhi Aerosol Supersite study, Atmos. Chem. Phys., 20, 8533–8549, https://doi.org/10.5194/acp-20-8533-2020, 2020.

Gierens, K. M., Lim, L., and Eleftheratos, K.: A review of various strategies for contrail avoidance. Open Atmospheric Science Journal, 2, 1-7, https://doi.org/10.2174/1874282300802010001, 2008.

Glovsky, M. M., Miguel, A. G., and Cass, G. R.: Particulate air pollution: possible relevance in asthma, Allergy Asthma Proc., 18, 163–166, https://doi.org/ 10.2500/108854197778965858, 1997.

Guenther, A., Karl, T., Harley, P., Wiedinmyer, C., Palmer, P. I., and Geron, C.: MEGAN: estimates of global terrestrial isoprene emissions, Atmos. Chem. Phys., 6, 3181–3210, https://doi.org/ 10.5194/acp-6-3181-2006, 2006.

Guo, S., Hu, M., Zamora, M. L., et al.: Elucidating severe urban haze formation in China. *Proceedings of the National Academy of Sciences*, *111*(49), 17373-17378, https://doi.org/10.1073/pnas.1419604111, 2014.

Heywood, J. B.: Internal Combustion Engine Fundamentals, 2nd ed., McGraw-Hill, New York, ISBN: 9781260116106, 2018.

Jacquot, O. and Sartelet, K.: Numerical investigations on ultrafine particle modelling in SSH-aerosol-v1.3a: size resolution and redistribution, Geosci. Model Dev., 18, 3965–3984, https://doi.org/10.5194/gmd-18-3965-2025, 2025.

Jeong, C.-H., Evans, G. J., McGuire, M. L., Chang, R. Y.-W., Abbatt, J. P. D., Zeromskiene, K., Mozurkewich, M., Li, S.-M., and Leaitch, W. R.: Particle formation and growth at five rural and urban sites, Atmos. Chem. Phys., 10, 7979–7995, https://doi.org/10.5194/acp-10-7979-2010, 2010.

Kelly, F. J. and Fussell, J. C.: Toxicity of airborne particles—established evidence and gaps, Phil. Trans. R. Soc. A, 378, 20190322, https://doi.org/ 10.1098/rsta.2019.0322, 2020.

Kim, Y., Shim, S., Cho, S., Yum, S. S., Song, C. H., and Park, S. H.: Improved estimation of new particle formation rate for an air-quality model in a polluted region of South Korea, Atmos. Environ., 121237, https://doi.org/ https://doi.org/10.1016/j.atmosenv.2025.121237, 2025.

Kirkby, J., Duplissy, J., Sengupta, K. et al.: Ion-induced nucleation of pure biogenic particles. Nature, 533(7604), 521-526, https://doi.org/10.1038/nature17953, 2016

Kohl, M., Lelieveld, J., Chowdhury, S., Ehrhart, S., Sharma, D., Cheng, Y., … Pozzer, A.: Global ultrafine particle

concentrations at the surface: simulations and evaluation, Atmos. Chem. Phys., 23, 13191–13215, https://doi.org/10.5194/acp-23-13191-2023, 2023.

Kulmala, M., and Laaksonen, A.: Binary nucleation of water–sulfuric acid system: Comparison of classical theories with different H2SO4 saturation vapor pressures. The Journal of Chemical Physics, 93(1), 696-701, https://doi.org/10.1063/1.459519, 1990

Kulmala, M., Laaksonen, A., and Pirjola, L.: Parameterizations for sulfuric acid/water nucleation rates. J. Geophys. Res., Vol 103, No D7, 8301-8307, https://doi.org/10.1029/97JD03718, 1998.

Kusaka, I., Wang, Z.-G., and Seinfeld, J. H.: Ion-induced nucleation: a density-functional approach, J. Chem. Phys., 102, 913–924, https://doi.org/ 10.1063/1.469408, 1995.

Lee, D. S., Pitari, G., Grewe, et al.: Transport impacts on atmosphere and climate: Aviation. Atmospheric environment, 44(37), 4678-4734, https://doi.org/10.1016/j.atmosenv.2009.06.005, 2010.

Lehtinen, K. E., Dal Maso, M., Kulmala, M., and Kerminen, V. M.: Estimating nucleation rates from apparent particle formation rates and vice versa: Revised formulation of the Kerminen–Kulmala equation. Journal of Aerosol Science, 38(9), 988-994, https://doi.org/10.1016/j.jaerosci.2007.06.009, 2007.

Leinonen, V., Kokkola, H., Yli-Juuti, T., Mielonen, T., Kühn, T., Nieminen, T., … Mikkonen, S.: Comparison of particle number size distribution trends in measurements and climate models, Atmos. Chem. Phys., 22, 12873–12905, https://doi.org/10.5194/acp-22-12873-2022, 2022.

Li, N., Chen, J.-P., Tsai, I-C., He, Q., Chi, S.-Y., Lin, Y.-C., Fu, T.-M.: Potential impacts of electric vehicle on Taiwan's air quality. Sci. Total Environ., 566-567, 919–928, https://doi.org/10.1016/j.scitotenv.2016.05.105, 2016a.

Li, N., Georas, S., Alexis, N., et al.: A work group report on ultrafine particles. (American Academy of Allergy, Asthma & Immunology): Why ambient ultrafine and engineered nanoparticles should receive special attention for possible adverse health outcomes in human subjects. Journal of Allergy and Clinical Immunology, 138(2), 386-396, https://doi.org/10.1016/j.jaci.2016.02.023, 2016b.

Lombaert, K., Le Moyne, L., De Maleissye, J. T., and Amouroux, J.: Experimental study of PAH in engine soot by isotopic tracing. Combustion science and technology, 178(4), 707-728, https://doi.org/10.1080/00102200500248417, 2006.

Mann, G. W., Carslaw, K. S., Ridley, D. A., et al..: Intercomparison of modal and sectional microphysics in the same 3-D model, Atmos. Chem. Phys., 12, 4449–4476, https://doi.org/ 10.5194/acp-12-4449-2012, 2012.

Mauderly, J. L.: Toxicological approaches to complex mixtures, Environ. Health Perspect., 101 (Suppl. 4), 155–165, https://doi.org/ 10.1289/ehp.93101s4155, 1993.

Mauderly, J. L.: Summary of the Third Colloquium on Particulate Air Pollution and Human Health, Air Pollution Health Effects Laboratory, Univ. of California, Irvine, 3-9–3-14, 1999.

Mosburger, M., Sick, V., and Drake, M. C.: Quantitative high-speed burned-gas temperature in engines using Na/K fluorescence, Appl. Phys. B, 110, 381–396, https://doi.org/10.1007/s00340-012-5290-9, 2013.

Napari, I., Kulmala, M., and Vehkamäki, H.: Ternary nucleation of inorganic acids, ammonia, and water. The Journal of

chemical physics, 117(18), 8418-8425, 2002. https://doi.org/10.1063/1.1511722

Oberdürster, G.: Toxicology of ultrafine particles: in vivo studies, Phil. Trans. R. Soc. A, 358, 2719–2740, https://doi.org/10.1098/rsta.2000.0680, 2000.

O'Dowd, C. D., Jimenez, J. L., Bahreini, R., Flagan, R. C., Seinfeld, J. H., Hämeri, K., ... and Hoffmann, T.: Marine aerosol formation from biogenic iodine emissions. Nature, 417(6889), 632-636, https://doi.org/10.1038/nature00775, 2002.

Park, S. K., Marmur, A., Kim, S.-B., Tian, D., Hu, Y., McMurry, P. H., and Russell, A. G.: Evaluation of fine PNC in CMAQ, Aerosol Sci. Technol., 40, 985–996, https://doi.org/10.1080/02786820600907353, 2006.

Patoulias, D. and Pandis, S. N.: Effects of low-volatility organics on aerosol number in Europe, Atmos. Chem. Phys., 22, 1689–1706, https://doi.org/10.5194/acp-22-1689-2022, 2022.

Petters, M. D. and Kreidenweis, S. M.: A single-parameter representation of hygroscopic growth and CCN activity, Atmos. Chem. Phys., 7, 1961–1971, https://doi.org/10.5194/acp-7-1961-2007, 2007.

Pope III, C.A., and Dockery, D.W.: Health effects of fine particulate air pollution: lines that connect. J Air Waste Manag. Assoc. 56(6):709-42, https://doi.org/10.1080/10473289.2006.10464485. PMID: 16805397, 2006.

Qi, X. M., Ding, A. J., Nie, W., Petäjä, T., Kerminen, V.-M., Herrmann, E., Xie, Y. N., Zheng, L. F., Manninen, H., Aalto, P., Sun, J. N., Xu, Z. N., Chi, X. G., Huang, X., Boy, M., Virkkula, A., Yang, X.-Q., Fu, C. B., and Kulmala, M.: Aerosol size distribution and new particle formation in the western Yangtze River Delta of China: 2 years of measurements at the SORPES station, Atmos. Chem. Phys., 15, 12445–12464, https://doi.org/10.5194/acp-15-12445-2015, 2015

Salma, I., Németh, Z., Kerminen, V.-M., Aalto, P., Nieminen, T., Weidinger, T., Molnár, Á., Imre, K., and Kulmala, M.: Regional effect on urban atmospheric nucleation, Atmos. Chem. Phys., 16, 8715–8728, https://doi.org/10.5194/acp-16-8715-2016, 2016.

Sartelet, K., Kim, Y., Couvidat, F., Merkel, M., Petäjä, T., Sciare, J., and Wiedensohler, A.: Influence of emission size distribution and nucleation on number over Greater Paris, Atmos. Chem. Phys., 22, 8579–8596, https://doi.org/10.5194/acp-22-8579-2022, 2022.

Skamarock, W. C., Klemp, J. B., Dudhia, J., Gill, D. O., Barker, D. M., Duda, M., … Powers, J. G.: A description of the Advanced Research WRF Version 3, NCAR Tech. Note TN-475+STR, 2008.

Schraufnagel, D. E.: The health effects of ultrafine particles, Exp. Mol. Med., 52, 311–317, https://doi.org/ 10.1038/s12276-020-0403-3, 2020.

Schwarz, M., Schneider, A., Cyrys, J., Bastian, S., Breitner, S., and Peters, A.: UFP and hospital admissions in three German cities, Environ. Int., 178, 108032, https://doi.org/ 10.1016/j.envint.2023.108032, 2023.

Shao, X., Wang, M., Dong, X., Liu, Y., Shen, W., Arnold, S. R., … Carslaw, K. S.: Global modeling of aerosol nucleation with HOM chemistry, Atmos. Chem. Phys., 24, 11365–11389, https://doi.org/ 10.5194/acp-24-11365-2024, 2024.

Shehata, M. S.: Cylinder pressure, heat release, and combustion duration for SI engines, Energy, 35, 4710–4725, https://doi.org/ 10.1016/j.energy.2010.09.033, 2010.

Sorokin, A., Katragkou, E., Arnold, F., Busen, R., and Schumann, U.: Gaseous SO_3 and H_2SO_4 in aircraft gas-turbine

exhaust: CIMS measurements and implications, Atmos. Environ., 38, 449–456, https://doi.org/10.1016/j.atmosenv.2003.10.054, 2004.

Spracklen, D. V., Carslaw, K. S., Merikanto, J., Mann, G. W., Reddington, C. L., Pickering, S., … Sun, J.: Explaining global surface aerosol number: primary emissions and formation, Atmos. Chem. Phys., 10, 4775–4793, https://doi.org/10.5194/acp-10-4775-2010, 2010.

Stafoggia, M., Michelozzi, P., Schneider, et al.: Joint effect of heat and air pollution on mortality in 620 cities, Environ. Int., 181, 108258, https://doi.org/10.1016/j.envint.2023.108258, 2023.

Ström, L., and Gierens, K.: First simulations of cryoplane contrails. Journal of Geophysical Research: Atmospheres, 107(D18), AAC-2, https://doi.org/10.1029/2001JD000838, 2002.

Tsai, I.-C., J.-P. Chen, Y.-C. Lin, C. C.-K. Chou, and W.-N. Chen: Numerical investigation of the coagulation mixing between dust and hygroscopic aerosol particles and its impacts, Journal of Geophysical Research: Atmospheres, 120, 4213–4233, https://doi.org/10.1002/2014JD022899, 2015a.

Tsai, I.-C., J.-P. Chen, C. S.-C. Lung, N. Li, W.-N. Chen, T.-M. Fu, C.-C. Chang, and G.-D. Hwang: Sources and formation pathways of organic aerosol in a subtropical metropolis during summer, Atmospheric Environment, 117, 51-60, https://doi.org/10.1016/j.atmosenv.2015.07.005, 2015b.

Tsai, I.-C., Lee, C.-Y., Lung, S. C. C., and Su, C.-W.: Vision-based traffic activity and urban air quality in Greater Taipei, Sci. Total Environ., 782, 146571, https://doi.org/ 10.1016/j.scitotenv.2021.146571, 2021.

Tuovinen, S., Cai, R., Kerminen, V.-M., Jiang, J., Yan, C., Kulmala, M., and Kontkanen, J.: Survival probabilities of atmospheric particles: comparison based on theory, cluster population simulations, and observations in Beijing, Atmos. Chem. Phys., 22, 15071–15091, https://doi.org/10.5194/acp-22-15071-2022, 2022.

Vehkamäki, H., Kulmala, M., Napari, I., Lehtinen, K. E., Timmreck, C., Noppel, M., and Laaksonen, A.:. An improved parameterization for sulfuric acid–water nucleation rates for tropospheric and stratospheric conditions. Journal of Geophysical Research: Atmospheres, 107(D22), AAC-3, https://doi.org/10.1029/2002JD002184, 2002

Wan, Y., Huang, X., Xing, C., Wang, Q., Ge, X., and Yu, H.: Chemical characterization of organic compounds involved in iodine-initiated new particle formation from coastal macroalgal emission, Atmos. Chem. Phys., 22, 15413–15423, https://doi.org/10.5194/acp-22-15413-2022, 2022.

Wang, K., Ma, X., Tian, R., and Yu, F.: New particle formation events vs. GEOS-Chem-APM in Beijing, Atmos. Chem. Phys., 23, 4091–4104, https://doi.org/ 10.5194/acp-23-4091-2023, 2023.

Westervelt, D. M., Pierce, J. R., Riipinen, I., Trivitayanurak, W., Hamed, A., Kulmala, M., Laaksonen, A., Decesari, S., and Adams, P. J.: Formation and growth of nucleated particles into cloud condensation nuclei: model–measurement comparison, Atmos. Chem. Phys., 13, 7645–7663, https://doi.org/10.5194/acp-13-7645-2013, 2013.

Whitby, K. T.: The physical characteristics of sulfur aerosols, Atmos. Environ., 12, 135–159, https://doi.org/ 10.1016/0004-6981(78)90196-8, 1978.

Xausa, F., Paasonen, P., Makkonen, R., Arshinov, M., Ding, A., Denier van der Gon, H., … Kulmala, M.: Advancing global

aerosol simulations with size-segregated anthropogenic number emissions, Atmos. Chem. Phys., 18, 10039–10054, https://doi.org/ 10.5194/acp-18-10039-2018, 2018.

Xu, W., Kuang, Y., Xu, W., Zhang, Z., Luo, B., Zhang, X., Tao, J., Qiao, H., Liu, L., and Sun, Y.: Hygroscopic growth and activation changed submicron aerosol composition and properties in the North China Plain, Atmos. Chem. Phys., 24, 9387–9399, https://doi.org/10.5194/acp-24-9387-2024, 2024.

Yu, F.: Chemiions and nanoparticle formation in diesel engine exhaust. Geophysical Research Letters, 28(22), 4191-4194, https://doi.org/10.1029/2001GL013732, 2001.

Yu, F., Lanni, T., and Frank, B. P.: Measurements of ion concentration in gasoline and diesel engine exhaust. Atmospheric Environment, 38(10), 1417-1423, https://doi.org/10.1016/j.atmosenv.2003.12.007, 2004.

Zieger, P., Väisänen, O., Corbin, J. C., Partridge, D. G., Bastelberger, S., Mousavi-Fard, M., … Salter, M. E.: Revising the hygroscopicity of inorganic sea-salt particles, Nat. Commun., 8, 15883, https://doi.org/10.1038/ncomms15883, 2017.